Efficient and ultrafast organic scintillators by hot exciton manipulation

Jiang Tang (jtang@mail.hust.edu.cn)
Wuhan National Laboratory for Optoelectronics (WNLO) and School of Optical and Electronic Information, Huazhong University of Science and Technology (HUST) https://orcid.org/0000-0003-2574-2943

Xinyuan Du
Huazhong University of Science and Technology

Shan Zhao
Huazhong University of Science and Technology

Lu Wang
Key Lab of OrganicOptoelectronicsand Molecular Engineering of Ministry of Education, Department of Chemistry, TsinghuaUniversity

Haodi Wu
Huazhong University of Science and Technology

Fan Ye
Wuhan National Laboratory for Optoelectronics& School of Optical and Electronic Information Huazhong University of Science and Technology

Kan-Hao Xue
Wuhan National Laboratory for Optoelectronics, Huazhong University of Science and Technology https://orcid.org/0000-0002-2894-7912

Shaoqian Peng
State Key Laboratory of Advanced Technology for Materials Synthesis and Processing, Center of Smart Materials and Devices, Wuhan University of Technology

Jianlong Xia
State Key Laboratory of Advanced Technology for Materials Synthesis and Processing, Center of Smart Materials and Devices, Wuhan University of Technology

Ziru Sang
Lauterbur Research Center for Biomedical Imaging, Shenzhen Institutes of Advanced Technology, Chinese Academy of Sciences

Dongdong Zhang
Tsinghua University https://orcid.org/0000-0002-8433-6200

Zuping Xiong
College of Chemistry and Life Science, Zhejiang Normal University

Zhiping Zheng

Huazhong University of Science and Technology

Ling Xu

Huazhong University of Science and Technology https://orcid.org/0000-0001-9676-5769

Guangda Niu

Wuhan National Laboratory for Optoelectronics (WNLO) and School of Optical and Electronic Information, Huazhong University of Science and Technology (HUST) https://orcid.org/0000-0002-9285-4147

Article

Keywords:

Posted Date: March 31st, 2023

DOI: https://doi.org/10.21203/rs.3.rs-2740655/v1

Additional Declarations: There is **NO** Competing Interest.

Version of Record: A version of this preprint was published at Nature Photonics on January 11th, 2024. See the published version at https://doi.org/10.1038/s41566-023-01358-y.

Abstract

Efficient and fast scintillators are in high demand for a variety of fields, such as medical diagnostics, scientific instruments, and high-energy physics. However, the trade-off between high scintillation efficiency and fast timing properties is a common challenge faced by almost all scintillators. To overcome this limitation, we have developed a new strategy for organic scintillators by directing all hot excitons into fast singlet emission states without involving the lowest triplet states. Our scintillator 1,1,2,2-tetraphenylethylene (4-bromophenyl) (TPE-4Br) shows an ultrafast radiative lifetime of 1.79 ns and ~ 72600 photons MeV^{-1} light yield, exhibiting an unprecedented combination of high light yield and short decay time. Our work provides a paradigm-shifting method to design efficient and ultrafast scintillators and paves the way towards exciting applications toward ultrafast detection and imaging.

Introduction

Scintillation is the process that ionizing radiation converts its energy into photons through the interaction of a material. It has widespread applications, including X-ray detection in radiological imaging and nondestructive inspection[1, 2], γ-ray detection in radioisotope identification and positron emission tomography (PET)[3, 4], beta ray detection in electron microscopes[5], and electromagnetic calorimeters in high-energy physics experiments[6, 7]. Development of scintillators with higher efficiency and faster timing properties is always the chasing goal of the field as high efficiency could generate more photons for a given radiation and produce better images without dosage increase, and fast scintillation enables quicker imaging and less lag, both of which are crucial for computed tomography (CT) and PET as well as high-energy physics application.

The study of inorganic scintillators has been ongoing for more than seventy years since the discovery of Sodium Iodide by Hofstadter in 1949.[7] Generally, inorganic scintillators have high efficiency (> 50000 photons MeV^{-1}) but inferior lifetime properties (tens of ns to thousands of ns) and thus limits their application with the urgent demand of fast scintillators (sub ns to ns) for high-energy physics and medical imaging.[8–11] Hence, organic scitllators have been studied due to their intristic fast lifetime (ns) as a result of the large electron-hole wave function overlap in molecular crystals. In addition, organic scintillators have advantages in low-temperature processing, abundant resourece supplies, high mechanical flexibility, and cost-effective fabrication in large volumes.[12] However, their performance is fundamentally limited by the inefficient exciton utilization and thus low radioluminescence efficiency (typically < 20000 photons MeV^{-1}), as well as small radiation stopping power inherent to their low atomic number. The low efficiency is due to that the weak spin-orbit coupling in conventional organic scintillators only generates fluorescence from singlet excitons upon high-energy X/γ-ray excitation, and approximately 75% triplet excitons relax primarily *via* non-radiative pathways. To circumvent these limitations, thermally activated delayed fluorescence (TADF) organic molecules and organic phosphors based on high-*Z* organometallics and halogenated organic materials have been extensively studied as organic scintillators to exploit the triplet excitons for emission recently.[13–15] Despite these increase the radioluminescence yield, the scintillation lifetime is unwantedly severely prolonged to microsecond or even second time scale

via the delayed fluorescence or phosphorescence process, which lose the intrinstic advantage of organic scintillators.

We propose a different approach to achieve undelayed fluorescence by manipulating the hot excitons and thus circumvent this dilemma of organic scintillators. Figure 1a schematically shows the interaction process between high-energy X/γ-rays and organic materials. X/γ-ray photons firstly transfer all or partial of their energy to the materials, producing primary high-energy electrons. These primary photoelectrons further collide with organic scintillators, releasing secondary high-energy electrons[16]. Then the interaction between the primary/secondary electrons and the organic molecules could lead to the removal of an electron completely from an atom (ionization) or to the promotion of an electron to a higher-lying shell (excitation)[17]. The excited electrons maintain the same spin state as the ground state electrons, forming only singlet excitons. The ionized electrons, which dominate the scintillation process, populate the excited states and consist of singlet and triplet excitons in the ratio of 1:3 following the rule of spin conservation.[14] In conventional organic scintillators and recently reported phosphorescent and TADF scintillators, the high-lying singlets and triplets would rapidly, within ps and driven by thermodynamics, relax to the lowest singlet (S_1) and triplet (T_1) states through internal conversion, respectively.[13–15] The occupation of spin forbidden T_1 states either creates non-radiative recombination channel in the case of conventional scintillators, as in anthracene, or prolongs decay time in phosphorescent and TADF scintillators. Thus, the key to realize efficient and fast organic scintillators is to exclude the occupation of T_1 states without sacrificing hot excitons. However, this dreaming process is fundamentally challenging and so far, to our best knowledge, there is no report on such hot exciton scintillators.

We analyze the possibility of manipulating all hot excitons into S_1 states without involving T_1 states. Fundamentally, in order to achieve the above effect, the hot excitons should relax from the higher triplet states (T_n) to the singlet states (S_m) and subsequent S_1 states *via* high-lying reverse intersystem crossing (hRISC), avoiding the population of T_1 states (Fig. 1a). To realize efficient hRISC, it is obligatory to suppress the internal conversion (IC) of $T_n \rightarrow T_1$ and accelerate the hRISC of $T_n \rightarrow S_m$. If the hRISC rate is sufficiently high, the IC could be completely suppressed, and all the high-energy triplet excitons could be converted to singlet excitons.[18] According to the photochemical theory, the rates of hRISC and IC are inversely proportional to the energy gap between the initial and final states. Therefore, for material screening, the S_1 and T_1 states of the targeted molecules should be localized exciton with large energy differences, and T_n and S_m should be delocalized excitons with small energy splitting.[19]

Following these rules here we have successfully developed a series of hot exciton scintillators (HES), which also contain heavy halogen atoms to enhance the X/γ-ray attenuation efficiency. Figure 1c presents three typical molecules, 1,1,2,2-tetrakis(4-bromophenyl)ethane (TPE-4Br), 1,1,2,2-tetrakis(3'-bromo-[1,1'-biphenyl]-4-yl)ethane (*m*-BrTBE) and benchmark organic scintillator anthracene. We compared the scintillator performance of TPE-4Br and *m*-BrTBE with representative organic and inorganic scintillators, as shown in Fig. 1b and Table S1. TPE-4Br (72600 photons MeV^{-1}, 1.79 ns) and *m*-BrTBE

(64500 photons MeV^{-1}, 1.33 ns) exhibits an unprecedented combination of high light yield and short decay time, showcasing the strength of hot exciton scintillators.

We now investigate the scintillation performance of the HES in detail. Figure 2a shows the X-ray absorption spectrum of the organic molecules in a broad range of X-ray photon energies from 1 to 1000 keV. It should be noted that the linear attenuation coefficient of photoelectric effect μ is determined by Z^4/E^3 (Z is the atomic number and E is the energy of X-ray photons or gamma ray photons). Due to the presence of heavy atom Br (Z = 35), the attenuation efficiency of TPE-4Br and *m*-BrTBE is much higher than that of anthracene across the whole energy region. The X-ray attenuation efficiency versus thickness of these materials for RQA3 spectrum is reported in Fig. S1. Obviously, a thickness of 1.34 mm is enough for TPE-4Br to attenuate 80% of the incident X-ray photons, while anthracene needs 54.46 mm. The X-ray excited radiation luminescence (RL) spectra of these organic molecules at room temperature are shown in Fig. 2b. In sharp contrast to anthracene with multiple emission peaks, TPE-4Br and *m*-BrTBE exhibit a single emission peak at 448 nm and 456 nm, respectively. Moreover, the peak shape and position of these organic molecules are almost identical to their photoluminescence (PL) spectrum (Fig. S2), indicating the singlet fluorescence nature of the radioluminescence. The transient photo luminescence (TRPL) of these organic molecules is shown in Fig. 2c. These curves are well-fitted by a single-exponential function. The time constant of TPE-4Br and *m*-BrTBE are 1.79 ns and 1.33 ns, respectively. Moreover, the photoluminescence quantum yields of TPE-4Br and *m*-BrTBE are as high as 93.7% and 61.7% (Fig. S3), respectively, demonstrating that the nonradiative recombination is negligible for these two molecules. In comparison, TADF material DMAC-TRZ and TADF-I exhibits long decay tail of 2150 ns and 1420 ns respectively, and the decay time of phosphorescent scintillator 9,9'-(6-iodophenoxy-1,3,5-triazine-2,4-diyl)bis(9H-carbazole) even reaches tens of ms.[14, 15]

Given the efficient absorption efficiency of TPE-4Br, we then selected it as a model to evaluate the steady-state X-ray to light conversion efficiency, lowest detectable dose rate and radiation hardness. To measure the emission intensity and obtain the light yield, TPE-4Br and anthracene powder are fabricated with different thicknesses (Table S2). Here we employ two separate methods for strictly evaluating the light yield, one is the X-ray excited steady radioluminescence intensity[20] and the other is the γ-ray excited pulse radioluminescence intensity (also known as pulse height spectrum)[21]. For the X-ray excited steady RL emission, one side of the scintillator is coupled onto a silicon photomultiplier (SiPM) and the other side is exposed to X-ray (Fig. S4). The light yield is calculated by correcting the wavelength-dependent detection efficiency (Fig. S5) of SiPM for scintillators. The corrected response amplitude of TPE-4Br and anthracene versus thickness is shown in Fig. 2d. Due to the large absorption efficiency, the steady RL intensity of TPE-4Br reaches saturation at a smaller thickness than anthracene. It is worth noting that the resolution and contrast of the image in practical X-ray imaging is directly determined by the steady RL intensity and thus we calculate the relative light yield by comparing the saturated RL intensity of TPE-4Br with that of anthracene. The saturated RL intensity of TPE-4Br is about 4.54 times larger than that of anthracene (16000 photons MeV^{-1}), which gives the equivalent light yield of TPE-4Br under X-ray excitation as 72600 photons MeV^{-1}. The light yield of *m*-BrTBE is also charactered as 64500

photons MeV^{-1} with the same method (Fig. S6). To derive the light yield under γ-ray, we recorded the pulse height spectrum of the organic scintillators toward ^{241}Am source (γ-ray: 59.5 keV) (Fig. S7). Fig. S8 shows the γ-ray pulse height spectrum. After correcting the wavelength-dependent detection efficiency of PMT for TPE-4Br and anthracene, the pulse height of TPE-4Br is estimated as 2.94 times larger than that of anthracene. The relatively small light yield of TPE-4Br under γ-ray may be due to the limited absorption capability of the pellets.

Additionally, the lowest detectable dose rate is a crucial parameter for the scintillator. Figure 2e shows the signal-to-noise ratio (SNR) versus irradiation dose rate. We record the lowest detectable dose rate of TPE-4Br as 109 $nGy_{air}\ s^{-1}$ at SNR = 3, which is four times lower than that of anthracene (447 $nGy_{air}^{-1}\ s^{-1}$) and 50 times smaller than the regular dose rate required in medical diagnostics (5.5 $\mu Gy_{air}\ s^{-1}$)[22], demonstrating its great potential in low dose radiation detection. As for the radiation stability, the TPE-4Br is continuously irradiated by the X-ray without any encapsulation. As shown in Fig. 2f, the light output of the TPE-4Br single crystal exhibits negligible degradation during continuous X-ray irradiation with a total dose of about 250 Gy_{air} at a high dose rate of 5.5 $mGy_{air}\ s^{-1}$ in ambient atmosphere (25 ^{o}C, 30% humidity).

To validate the above claimed hot-exciton harvesting mechanism, the geometrical and electronic structures of TPE-4Br is calculated. The results are shown in Fig. 3a (more information is in Fig. S9 and Table S3). The highest occupied molecular orbital (HOMO) and lowest unoccupied molecular orbital (LUMO) almost spread over the whole molecule skeleton. The singlet and the triplet energies are calculated based on TD-DFT method with Tamm-Dancoff approximation with singlet energy levels as S_1 (2.70 eV), S_2 (3.60 eV), and triplet energy levels as T_1 (1.49 eV), T_2 (3.06 eV), T_3 (3.14 eV), T_4 (3.42 eV) and T_5 (3.55 eV). Moreover, the calculated energy of S_1 (2.70 eV) well matched the PL spectrum of TPE-4Br powder (peak at 448 nm), demonstrating the accuracy of theoretical calculation. Obviously, the energy gap between T_2 and T_1 is as large as 1.57 eV, while that between S_2 and T_5-T_2 is relatively small (0.05 eV, 0.18 eV, 0.46 eV, 0.54 eV, respectively). Thus, the TPE-4Br indeed has a large T_n-T_1 energy gap and a small T_n-S_m energy splitting, which is necessary to suppress the internal conversion of T_n to T_1 and accelerate the hRISC of T_n to S_m. Furthermore, according to the perturbation theory, the rate of ISC and hRISC, k_{ISC} and k_{RISC}, is determined by the energy gap ($\triangle E_{ST}$) and the spin-orbit coupling (SOC) constant (ξ_{ST}) between the involved triplet and singlet states, and can be expressed by the formula[23]:

$$k_{ISC/RISC} \propto \frac{{\xi_{ST}}^2}{e^{\triangle {E_{ST}}^2}}$$

The SOC strengths between S_1 and T_1-T_5 are calculated as 0.54 cm^{-1}, 6.22 cm^{-1}, 9.38 cm^{-1}, 2.11 cm^{-1}, 5.21 cm^{-1} (Table S4), respectively. Obviously, the SOC strength between S_1 and T_2-T_5 is much larger than that between S_1 and T_1. The stronger SOC strength as well as smaller energy gap between S_1 and T_2-T_5 of TPE-4Br together guarantee the considerable hRISC rate from T_n to S_m.

Furthermore, from the experimental view, there are two processes need to be identified to validate the hot-exciton harvesting mechanism: (1) fast hRISC process and (2) negligible ISC efficiency from S_1 to T_1. To verify the fast hRISC process, we directly use a sensitizer to populate only the high triplet states (T_n) of TPE-4Br. If the high triplet states (T_n) of TPE-4Br relax to T_1 state, we then could observe phosphorescence or delayed fluorescence with long lifetime. Otherwise, the high triplet states of TPE-4Br take the relaxation channel to S_1 state through the fast hRISC process. Here benzophenone (BP) is chosen as the sensitizer and has a well-known T_1 state level of 3.01 eV,[24] which is very close to the T_2 state (3.06 eV) of TPE-4Br. The matched energy level and spin state guarantees the successful population of T_2 states. The inset of Fig. 3b shows the PL spectrum of the pure TPE-4Br (T) solution and the TPE-4Br solution sensitized by BP (TB). There is negligible difference of PL spectrum shape and the peak position (473 nm) for T solution and TB solution, indicating that the luminescence of the two solutions originates from the same S_1 radiative channel of TPE-4Br. The PL decay profiles of the T solution and TB solution at room temperature with an excitation wavelength of 340 nm are shown in Fig. 3b. Both solutions demonstrate a fast decay time of 0.96 ns for T solution and 1.44 ns for TB solution, which is identified as the the S_1 state emission of TPE-4Br. In addition to the fast decay time, the TB solution exhibits another slightly slow decay time of 4.56 ns, which is originated from the sensitizing process from BP to TPE-4Br. Anyway, there is no long lifetime component for phosphorescence or delayed fluorescence, confirming the fast hRISC process in TPE-4Br. The illustration of the photo-physical processes existing in the TPE-4Br solutions with BP are shown in Fig. S10.

Subsequently, we adopt the previously established transient absorption method to evaluate negligible ISC from S_1 to T_1 of TPE-4Br.[25, 26] We prepared TPE-4Br and benzil (reference) solutions. β-carotene was added to both TPE-4Br and benzil solutions. TPE-4Br and benzil could serve as the triplet exciton donors to sensitize β-carotene. β-carotene is selected because the negligible excitation by the selected pump wavelength (343 nm) and its well-known insignificant ISC ($_{isc} \approx 0$). Thereby, the observation of triplet emission of β-carotene could directly reflect the occupation of T_1 states of the sensitizer. The illustration of the photo-physical processes in the solutions with and without β-carotene is shown in Fig. S11. For the solutions without β-carotene, after the excitation of donors (TPE-4Br or benzil), the excitons are populated to S_1 state, and then some of the S_1 state excitons could transfer to the T_1 state by ISC process. In pump-probe spectra, it is possible to observe the S_1-S_n and T_1-T_n transient absorption of the donors. As shown in Fig. S12, we indeed observed two photo absorption (PA) features at 529 nm and 487 nm for the pure benzil solutions without β-carotene, where the PA signal at 529 nm (life time: 2.39 ns) is originated from the S_1-S_n process[27] and that at 487 nm[28] (life time: 2.62 μs) is ascribed to the T_1-T_n process of benzil. The same process also occurs in TPE-4Br solutions, but we only observed one PA features at 458 nm (life time: 1.39 ns), which is originated from the S_1-S_n process (Fig. S13). For the solutions with β-carotene addition, the T_1 excitons of the donors (TPE-4Br or benzil) could principlly sensitize T_1 state of the acceptor (β-carotene). Therefore, there will be the additional PA signal caused by T_1-T_n transient absorption of the acceptors. We can see an additional PA features at 519 nm of benzil solutions with β-carotene, which is ascribed to the T_1-T_n process of β-carotene (Fig. 3c and Figure S14).[29] However, there

is still only one PA signal features at 458 nm for TPE-4Br solutions with β-carotene. The absence of T_1 state PA signal in both TPE-4Br solutions with and without β-carotene strongly testifies the negligible ISC process form S_1 to T_1 in TPE-4Br.

In addition to the effective hRISC and negligible S_1-T_1 ISC processes, the fluorescence efficiency (S_1-S_0) is also very important to guarantee the scintillation yield. Commonly, the halogen atoms of organic materials can lead to the enhancement of phosphorescence and the quenching of the fluorescence by promoting the ISC process from S_1 to T_1 (also known as heavy-atom effect).[30] We then measured the fluorescence efficiency of TPE-4Br and its parent molecule without bromide TPE (the molecular structure is shown in Fig. S16a) at room temperature by an absolute photoluminescence measurement system with an integrating sphere. The fluorescence efficiency of TPE-4Br and TPE are 93.7% and 60.5% via calculation of emission divided by absorbance (Fig. S16b). To our surprise, the introduction of bromine atoms in TPE-4Br exhibits improved emission efficiency compared to TPE. The anomalous anti-heavy-atom effect of TPE-4Br is quite different from the traditional heavy-atom effect. As TPE-4Br has the properties of aggregation-induced emission (AIE), we also calculate the density of states (DOS) for TPE-4Br as shown in Fig. 3e, the valence band maximum (VBM) and conduction band minimum (CBM) are both derived from the carbon atoms with little contribution from the hydrogen and bromine atoms, consistent with the calculation results of HOMO and LUMO. As a result, the heavy bromine atoms do not contribute to the S_1-T_1 ISC process. More importanly, the presence of Br in TPE-4Br molecule also results in some additional strong intermolecular forces. The Hirshfeld surface mapped over density of normal distribution (d_{norm}) and decomposed fingerprint plots of TPE-4Br and TPE are shown in Fig. 3f and Fig. S17. The intermolecular interactions of Br···H and Br···Br bonds can be easily found in TPE-4Br molecules with ordered packing pattern in the crystal structure. The proportion of Br···H and Br···Br interaction to total intermolecular interaction are 37.2% and 9.9% respectively, playing important roles in the intermolecular interactions among TPE-4Br molecules. The presense of the hydrogen bonding and halogen bonding is responsible for the restriction of intermolecular motions and thus suppression of the phonon-mediated emission quenching.

Efficient and ultrafast detection of X/γ-rays plays an important role in medical imaging, flash X-ray radiography and high-energy physics (Fig. 4a).[31–33] For example, as a result of relying on the time of flight (TOF) technique, fast scintillators are critical for PET and CT to get better temporal resolution.[34.35] Moreover, scintillators with ultrafast decay time have the capability to distinguish almost simultaneous events and mitigate the pile-up effect (Fig. 4b), which is vital in flash X-ray radiography and high-energy physics. The luminescence decay curve (X-ray pulse excited) of TPE-4Br is shown in Fig. 4c and the decay time is fitted as 1.32 ns, consistent with the photoluminescence decay time (1.79 ns). We demonstrate the high resolution and flash X-ray imaging capability by TPE-4Br scintillators. The X-ray imaging system is constructed with a digital camera, a reflector and the Amptek Mini X-ray tube (Fig. S18). To fabricate a large scintillator film, we mixed the TPE-4Br molecules into sucrose octaacetate (SO) to obtain a plastic scintillator screen. We optimized the solubility as 1.7 wt% of TPE-4Br in SO matrix (Fig. 4d: top left) for later imaging. The X-ray image of an opaque capsule with a built-in metal spring clearly

shows the internal structure (Fig. 4d: top right). The bottom of Fig. 4d shows the image of a standard X-ray resolution pattern and indicates that the line pair notches at ~ 20.0 lp mm^{-1} could be well resolved. Furthermore, the modulation transfer function (MTF) curve (Fig. 4e) is obtained by adopting the slanted-edge method (Fig. S19). The spatial resolution at MTF = 0.2 of TPE-4Br scintillator, commercial CsI:Tl film and $Gd_2O_2S_2$:Tb (GOS) film are 18.69 lp mm^{-1}, 4.82 lp mm^{-1} and 2.78 lp mm^{-1}, respectively. The high spatial resolution exceeds most scintillator screens (Table S5) and is ascribed to the uniformly distributed refractive index and weak optical scattering of the transparent scintillator screen. In addition, we also characterized the normalized noise power spectra (NNPS) of TPE-4Br scintillator (Fig. 4f), which is almost flatten and outperforming commercial scintillators (TPE-4Br: 10^{-4} mm^2, CsI:Tl: 10^{-3} mm^2),[36] indicating the small cross-talk between neighbouring pixels. Figure 4g shows the flash X-ray imaging of the scintillator screen. The fusion process of bubbles in the saturated solution of lead based compounds (0.6 g $MAPbI_3$ in 1 mL γ-butyrolactone) could be clearly recorded by our high-speed imaging facility. The frame rates reach 10000 frame per second (fps). The right of Fig. 4g exhibits the specific merging process of two bobbles. The video of the mobile bubbles process is in Supplementary Information Movie 1. We note that considering the decay time constant of TPE-4Br, the imaging speed could be even increased to 10^8 fps, and the frame rates of the current system is restricted by the image camera. The ultrafast imaging could provide significant information for interior, intermediate, exterior and terminal ballistics and detonation research applications, as well as validating computer models and determining material parameters in transient interactions.

We also investigate the potential utility of TPE-4Br for PET imaging. The ultra-short pulse of the TPE-4Br crystals is of great benefit to time-of-flight PET (TOF-PET) which is a definite trend toward reducing image noise and improving the identification of cancerous lesions. To evaluate the coincidence time resolution (CTR) of the TPE-4Br crystals, we recorded the event data with two TPE-4Br based detectors (Fig. 4h). Figure 4i shows typical waveforms of coincidence pulse pair from the two detectors. We calculate the time difference (Δt) for 10,000 coincidence events and plot the histogram. Through the same way, we acquire the waveforms and the histogram of LYSO, which is commercially used for present PET system. The CTRs for TPE-4Br and LYSO, which are determined from Gaussian fitting to the data (Fig. 4j), are calculated to be 180 ps and 270 ps (full width at half maximum), respectively. The CTR obtained with TPE-4Br crystals is much better than the commercial PET scintillator LYSO, implying the ability to diagnose smaller lesions or tumors according to the formula in the inset of Fig. 4i.

In conclusion, we have developed a new family of hot-exciton scintillators to achieve efficient and ultrafast radioluminescence. The large energy gap between high-lying and lowest triplet state (T_n-T_1, $n \geq 2$), small energy splitting between high-lying triplet and singlet states (T_n-S_m, $n \geq 2$, $m \geq 1$), and strong spin-orbit coupling between S_1 and T_n ($n \geq 2$) facilitates the fully harvesting of radiation-induced hot excitons into the fast radiative S_1 state without population of T_1 state. Our strategy provides a solution to overcome the intrinsic dilemma between high scintillation efficiency and fast timing properties of scintillators, and our hot-exciton scintillator TPE-4Br shows a balanced performance outperforming nearly all existing scintillators. Our finding not only provides a paradigm-shifting approach for organic

scintillator design, but also broaden the utility of organic scintillators in various ultrafast radiation detection applications.

Declarations

Acknowledgments

This work was supported by the Major State Basic Research Development Program of China (2021YFB3201000, 2018YFA0703200), National Natural Science Foundation of China (62134003, 62074066, 62204092, 12050005), CAS Project for Young Scientists in Basic Research (YSBR-024), Fund for the Natural Science Foundation of Hubei Province (2021CFA036, 2020CFA034), and Shenzhen Basic Research Program (JCYJ20200109115212546), the HCP Program for HUST and the Innovation Fund of WNLO.

Author contributions

J.T. and G.N. supervised the whole project. X.D., S.Z. and H.W. carried out most material characterizations and device optimizations. L.W., F.Y., K.X., and D.Z. performed the theoretical simulation and analyzed the results. S.P. and J.X. carried out transient absorption characterizations. Z.S performed the coincidence time resolution measurements and analyzed the results. Z.Z. and L.X. assisted in data analysis. J.T., G.N. and D.X. wrote the paper; all authors commented on the manuscript.

Additional Information

Supplementary information is available in the online version of the paper. Reprints and permissions information is available online at www.nature.com/reprints.

Competing interests

The authors declare no competing financial interests.

References

1. C Roques-Carmes et al., A framework for scintillation in nanophotonics. *Science* **375**, 837 (2022).
2. Q Chen et al., All-inorganic perovskite nanocrystal scintillators. *Nature* **561**, 88-93 (2018).
3. SI Ziegler, Positron emission tomography: principles, technology, and recent developments. *Nuclear Physics A* **752**, 679C-687C (2005).
4. M Gandini et al., Efficient, fast and reabsorption-free perovskite nanocrystal-based sensitized plastic scintillators. *Nature Nanotechnology* **15**, 462-468 (2020).
5. Autrata R, Schauer P, Kuapil J, A single crystal of YAG-new fast scintillator in SEM. *J. Phys. E: Sci. Instr.* **11**, 707 (1978).

6. Fabjan C W, Ludlam T W, Calorimetry in high-energy physics. *Annu. Rev. Nucl. Part. Sci.* **32**, 335-389 (1982).
7. A Gektin, M Korzhik, Inorganic scintillators for detector systems (Springer, 2017).
8. P Lecoq et al., Scintillation and inorganic scintillators. *Inorganic scintillators for detector system: physical principles and crystal engineering* **1**, 1-41 (2017).
9. Lecoq P, Development of new scintillators for medical applications. *Nucl. Instrum. Methods Phys. Res. A* **809**, 130-139 (2016).
10. Kumar V, Luo Z, A review on x-ray excited emission decay dynamics in inorganic scintillator materials. *Photonics* **8**, 71 (2021).
11. ML Zaffalon et al., Extreme γ-ray radiation hardness and high scintillation yield in perovskite nanocrystals. *Nat. Photonics* **16**, 860-868 (2022).
12. TJ Hajagos, C Liu, NJ Cherepy, QB Pei, High-Z sensitized plastic scintillators: a review. *Adv. Mater.* **30**, 1706956 (2018).
13. X Wang et al., Organic phosphors with bright triplet excitons for efficient X-ray-excited luminescence. *Nat. Photonics* **15**, 187-192 (2021).
14. W Ma et al., Thermally activated delayed fluorescence (TADF) organic molecules for efficient X-ray scintillation and imaging. *Nat. Materials* **21**, 210-216 (2022).
15. JX Wang et al., Heavy-atom engineering of thermally activated delayed fluorophores for high-performance X-ray imaging scintillators. *Nat. Photonics* **16**, 869-875 (2022).
16. JB Birks, Scintillations from organic crystals: specific fluorescence and relative response to different radiations. *Proc. Phys. Soc. A* **64**, 874 (1951).
17. FD Brooks, Development of organic scintillators. *Nucl. Instrum. Methods Phys. Res* **162**, 477-505 (1979).
18. Y Pan et al., High yields of singlet excitons in organic electroluminescence through two paths of cold and hot excitons. *Adv. Optical Mater.* **2**, 510-515 (2014).
19. Y Xu, P Xu, D Hu, YG Ma. Recent progress in hot exciton materials for organic light-emitting diodes. *Chem. Soc. Rev.* **50**, 1030-1069 (2021).
20. R Turtos, S Gundacker, S Omelkov, E Auffray, P Lecoq, Light yield of scintillating nanocrystals under X-ray and electron excitation. *J. Lumin.* **215**, 116613 (2019).
21. VB Mykhaylyk, H Kraus, M Saliba, Bright and fast scintillation of organolead perovskite $MAPbBr_3$ at low temperatures. *Mater. Horiz.* **6**, 1740-1747 (2019).
22. I Clairand et al., Use of active personal dosemeters in interventional radiology and cardiology: Tests in laboratory conditions and recommendations-ORAMED project. *Radiat. Meas.* **46**, 1252-1257 (2011).
23. Zhao W et al., Highly sensitive switching of solid-state luminescence by controlling intersystem crossing. *Nat. Commun.* **9**, 1-8 (2018).

24. Y Xu et al., Highly efficient blue fluorescent OLEDs based on upper level triplet–singlet intersystem crossing. *Adv. Mater.* **31**, 1807388 (2019).
25. HD Burrows, M Fernandes, JS Melo, AP Monkman, SJ Navaratnam. Characterization of the triplet state of tris (8-hydroxyquinoline) aluminium (III) in benzene solution. *J. Am. Chem. Soc.* **125**, 15310-15311 (2003).
26. S Hirata, Intrinsic analysis of radiative and room-temperature nonradiative processes based on triplet state intramolecular vibrations of heavy atom-free conjugated molecules toward efficient persistent room-temperature phosphorescence. *J. Phys. Chem. Letters* **9**, 4251-4259 (2018).
27. N Ikeda, M Koshioka, H Masuhara, K Yoshihara, Picosecond dynamics of excited singlet states in organic microcrystals: Diffuse reflectance laser photolysis study. *Chem. Phys. Letters* **150**, 452-6 (1988).
28. PB Merkel, JP Dinnocenzo, Thermodynamic energies of donor and acceptor triplet states. *J. Photochem. Photobiol. A* **193**, 110-121 (2008).
29. S Bachilo, β-carotene triplet state absorption in the near-IR range. *J. Photochem. Photobiol. A* **91**, 111-115 (1995).
30. GG Giachino, DR Kearns. Nature of the external heavy-atom effect on radiative and nonradiative singlet–triplet transitions. *J. Chem. Phys.* **52**, 2964-2974 (1970).
31. P Russo, Handbook of X-ray imaging: physics and technology. (CRC press, 2017).
32. E Auffray et al., Crystal conditioning for high-energy physics detectors. *Nucl. Instrum. Methods Phys. Res. A* **486**, 22-34 (2002).
33. BV Ramudu, CJ Reddy, V Madhu, Flash X-ray radiography technique to study the high velocity impact of soft projectile on E-glass/epoxy composite material. *Def. Technol.* **15**, 216-226 (2019).
34. P Lecoq, Pushing the limits in time-of-flight PET imaging. *IEEE Trans. Radiat. Plasma Med. Sci.* **1**, 473-485 (2017).
35. R Turtos et al., Ultrafast emission from colloidal nanocrystals under pulsed X-ray excitation. *J. Instrum.* **11**, P10015 (2016).
36. RB Benitez, R Ning, D Conover, SH Liu, Measurements of the modulation transfer function, normalized noise power spectrum and detective quantum efficiency for two flat panel detectors: a fluoroscopic and a cone beam computer tomography flat panel detectors. *J. X-Ray Sci. Technol.* **17**, 279-293 (2009).

Figures

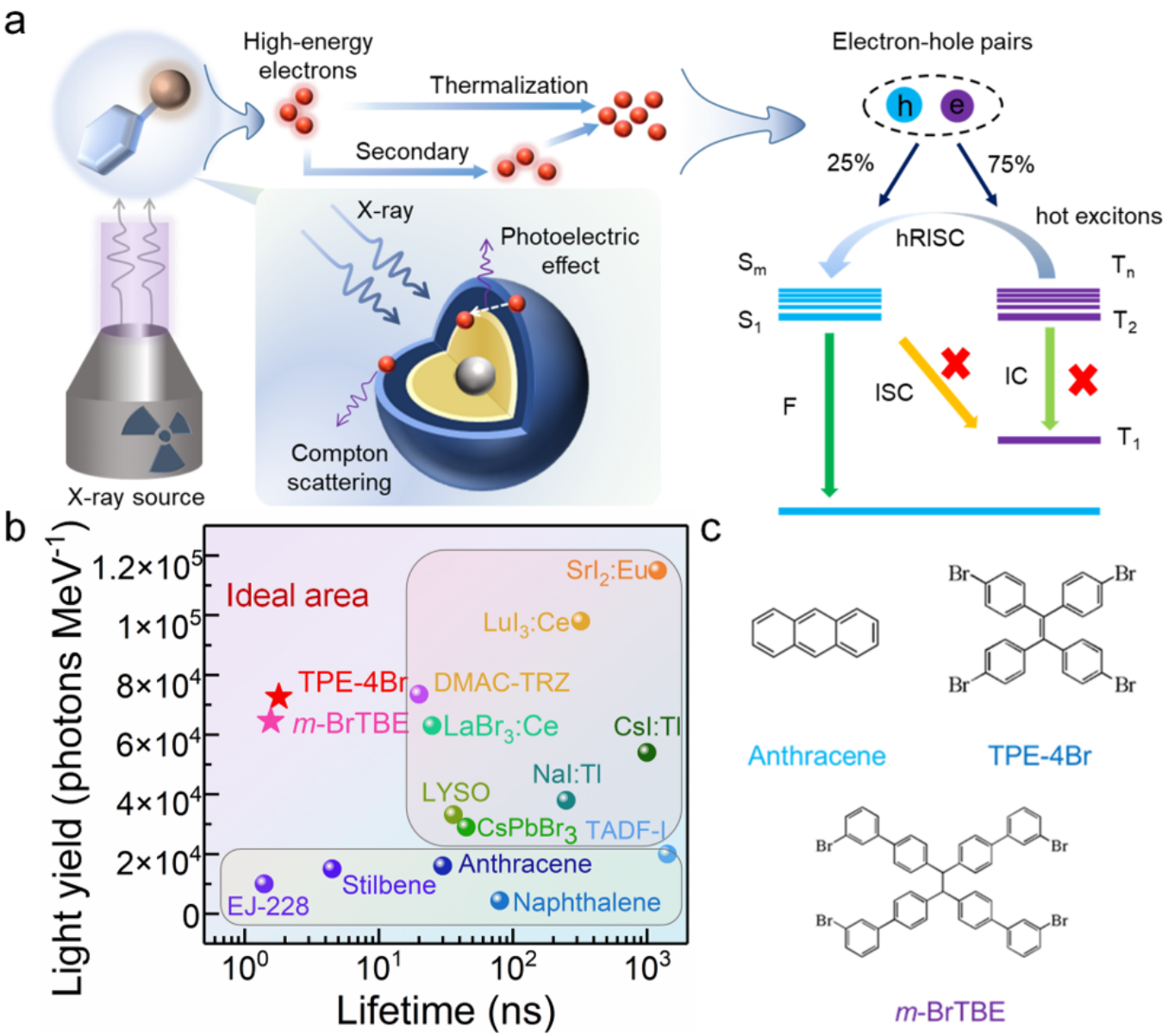

Figure 1

a) Schematic illustration of the X-ray induced scintillation process in hot exciton scintillator (HES). hRISC, high-lying reverse intersystem crossing; IC, internal conversion, S, singlet excitons; T, triplet excitons. b) Comparison of the HES with representative organic and inorganic scintillators in terms of light yield and lifetime. c) Molecular structures of two representative hot exciton scintillators (TPE-4Br, *m*-BrTBE), and conventional organic scintillator anthracene.

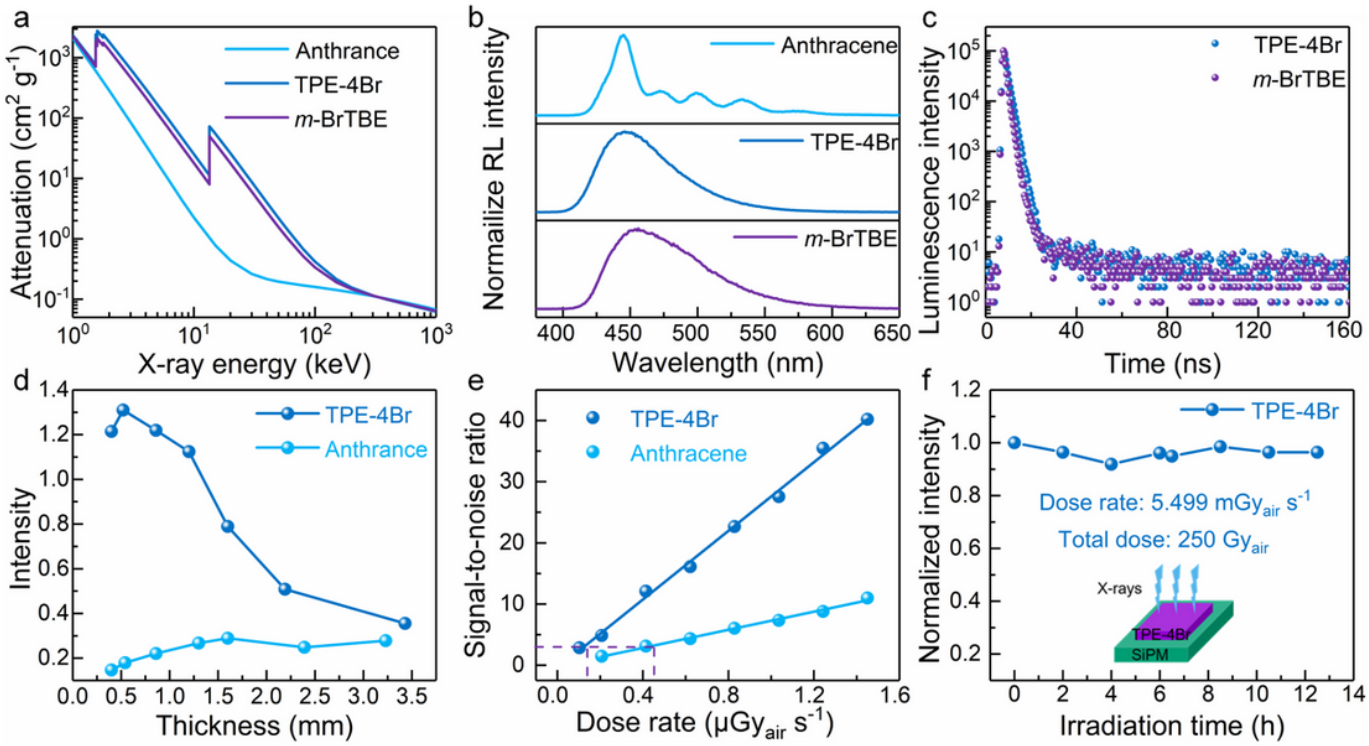

Figure 2

a) Attenuation coefficients of anthracene, TPE-4Br and *m*-BrTBE as a function of photon energy from 1 keV to 1000 keV. b) Normalized radioluminescence spectra of anthracene, TPE-4Br and *o*-BrTBE. c) Time-resolved PL decay spectrum of TPE-4Br and *m*-BrTBE at room temperature. Both of the decay curves can be well fitted by a single exponential function. d) The radiation luminescence intensity *versus* thickness of anthracene and TPE-4Br. e) The signal-to-noise ratio of TPE-4Br and anthracene to dose rate. f) Normalized emission intensity of TPE-4Br powders under continuous X-ray irradiation (X-ray tube voltage, 50 kV; dose rate: 5.5 mGy_{air} s^{-1}) for a total dose of 250 Gy_{air}.

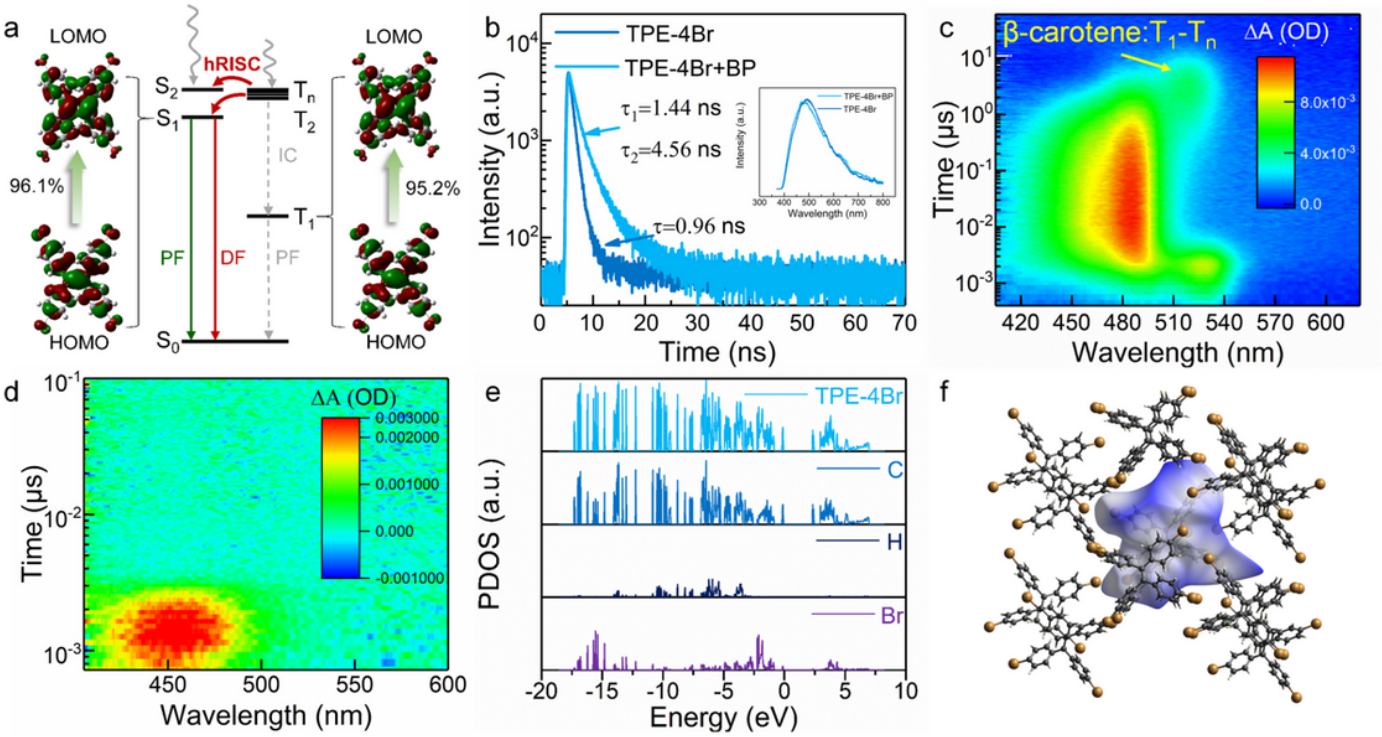

Figure 3

a) Energy-level diagrams and the normal modes of vibration of the molecular crystals for the singlet and triplet excited states of TPE-4Br. PF, prompt fluorescence, DF, delayed fluorescence. b) The PL decay spectra and PL spectra (inset) of TPE-4Br and TPE-4Br+BP solutions at room temperature. c and d) The two-dimensional contour plot of the transient absorption (TA) spectra of benzil solutions with β-carotene (c) and the TPE-4Br solutions with β-carotene (d). e) Density of states (DOS) of TPE-4Br and the contribution of C, H and Br element. f) A view of the Hirshfeld surface mapped over d_{norm} for TPE-4Br.

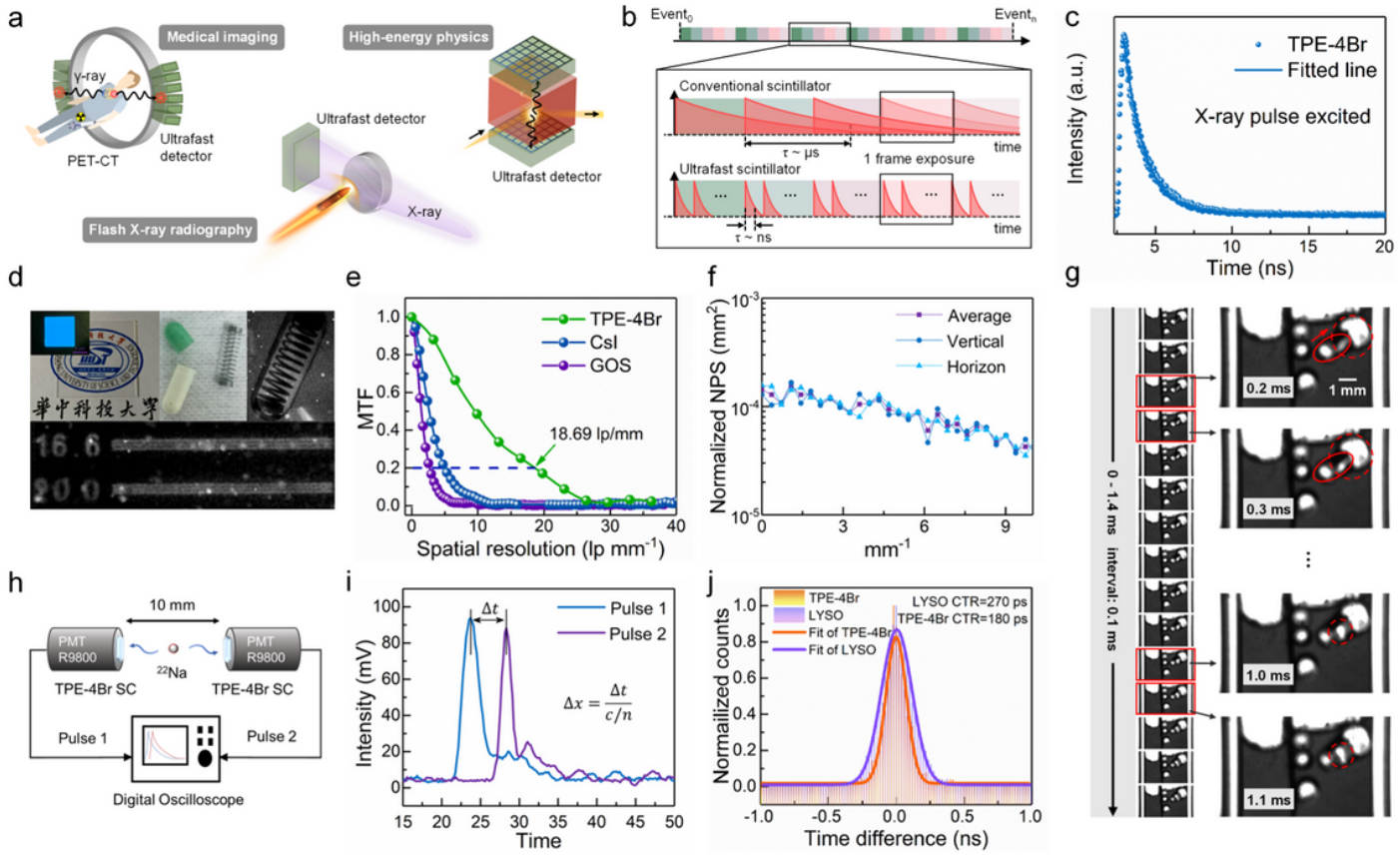

Figure 4

a) The application of the ultrafast scintillator in medical imaging (PET and CT), flash X-ray radiography and high-energy physics. b) The diagram of flash imaging of conventional and ultrafast scintillators. c) The luminescence decay curve of TPE-4Br with the excitation of X-ray pulse. d) Top left: photograph of the TPE-4Br scintillator screen without and with radiation excitation. Top right: optical and X-ray image of an encapsulated metallic spring. Bottom: X-ray image of the standard X-ray resolution pattern plate. e) MTF curves of the TPE-4Br scintillator screen. f) The normalized noise power spectra (NNPS) of TPE-4Br scintillator was measured at 2.5 μGy s^{-1}. g) The flash imaging of the bubbling process in solution by TPE-4Br scintillator screen. h) Schematic illustration of the coincidence time resolution (CTR) measurement. i) The decay curves collected by the two opposite detectors, and the location can be calculated based on the time difference as $\Delta x=\Delta T/(c/n)$. j) The measured photopeak selection with resulting delay time histogram and Gaussian fit giving the CTR values of TPE-4Br and LYSO.

Supplementary Files

This is a list of supplementary files associated with this preprint. Click to download.

- video3.mp4
- SI20230228.docx